ARTICLES

Journal of Semiconductors
(2020) 41, 012302
doi: 10.1088/1674-4926/41/1/012302

Realization of high-performance tri-layer graphene saturable absorber mirror fabricated via a one-step transfer process

Cheng Jiang[1, 5], Xu Wang[1], Jian Liu[1], Jiqiang Ning[2], Changcheng Zheng[3], Xiaohui Li[4], and Ziyang Zhang[1, †]

[1]Key Laboratory of Nanodevice and Applications, Suzhou Institute of Nano-Tech and Nano-Bionics, Chinese Academy of Sciences, Suzhou 215123, China

[2]Vacuum Interconnected Nanotech Workstation, Suzhou Institute of Nano-Tech and Nano-Bionics, Chinese Academy of Sciences, Suzhou 215123, China

[3]Division of Natural and Applied Sciences, Duke Kunshan University, Kunshan 215316, China

[4]School of Physics and Information Technology, Shaanxi Normal University, Xi'an 710119, China

[5]Nano Science and Technology Institute, University of Science and Technology of China, Suzhou 215123, China

Abstract: Graphene, as a saturable absorber (SA), has attracted much attention for its application in ultrashort pulse fiber lasers due to its ultrafast interband carrier relaxation and ultra-broadband wavelength operation. Nevertheless, during the stacking process of monolayer graphene layer, the induced nonuniform contact at the interface of graphene layers deteriorate the device performance. Herein, we report the fabrication of graphene saturable absorber mirrors (SAMs) via a one-step transfer process and the realization of the much enlarged modulation depth and the much reduced nonsaturable loss with tri-layer graphene (TLG) than single-layer graphene (SLG) due to the improved uniform contact at the interface. Moreover, the operation of 1550 nm mode-locked Er-doped fiber laser with the TLG SAM exhibits excellent output characteristics of the maximum output power of 9.9 mW, a slope efficiency of 2.4% and a pulse width of 714 fs. Our findings are expected to pave the way toward high-performance ultrashort pulse fiber lasers based on graphene SAs.

Key words: graphene; SAMs; mode-locked lasers; nonlinear absorption characteristics

Citation: C Jiang, X Wang, J Liu, J Q Ning, C C Zheng, X H Li, and Z Y Zhang, Realization of high-performance tri-layer graphene saturable absorber mirror fabricated via a one-step transfer process[J]. *J. Semicond.*, 2020, 41(1), 012302. http://doi.org/10.1088/1674-4926/41/1/012302

1. Introduction

Owing to the advantages of high beam quality, high reliability, efficient heat dissipation and compact size, pulse fiber laser shave widespread applications in both the scientific research and the industrial manufacture, including the optical communication, the spectroscopy, the sensing, materials and the signal processing[1–4]. Up to now, many studies of pulse fiber lasers have been conducted using active and passive mode locking methods[5–7]. In comparison with the active mode-locking, the passive mode-locking has the advantages of low cost and compactness[8]. Furthermore, it also exhibits the ability to produce transform-limited pulses without the need to employ any external active devices such as modulators. As a key element in passive mode-locked fiber lasers (PMLFLs), saturable absorbers (SAs) can effectively convert the continuous-wave operation into the pulsed operation because of their high absorption for low optical intensities and low optical absorption for the high optical intensity[9–13].

In recent years, carbon materials including carbon nanotubes (CNT) and graphene are emerged as effective SAs for constructing PMLFLs due to their low saturable intensity, ultrafast recovery time, and simple manufacturing processes[14]. The bandgap of CNT depends on the diameter of nanotube, thus, defining the operating wavelength[15]. Nevertheless, it is very difficult to obtain nanotubes with uniform diameter distribution in one SA for the saturable absorption of a particular wavelength of light, which induces much insertion losses. Therefore, the further development of the CNT-based PMLFLs are severely hindered. Compared to the CNT, the graphene has the major advantage of intrinsic wideband operation from the ultraviolet to the far-infrared region. Moreover, the excited carriers in pristine graphene exhibit ultrafast decay due to the zero bandgap in graphene[16–18]. Therefore, graphene has been chosen as one of the promising SA candidates. After the first demonstration of graphene SAs (G-SAs) in 2009[19], extensive studies have been conducted on G-SAs for ultrafast pulse generation in 1550 nm range. However, the graphene has ripples or corrugations due to thermal fluctuations, leading to the induced loose contact between neighbor layers during the stacking process of multilayer G-SAs. Moreover, the most of previous works only studied the effect of the number of graphene layer on the nonlinear absorption characteristics of G-SAs, but ignored the influence on the output characteristics of G-SAs based PMLFLs.

In this work, in order to study the effect of nonuniform contact at the interface of graphene layers, we have fabricated the single-layer graphene (SLG) and the tri-layer graphene (TLG) saturable absorber mirrors (SAMs) via a one-step transfer process. We investigate the optical nonlinearities of SLG and TLG SAMs. It has been found that the TLG-

Correspondence to: Z Y Zhang, zyzhang2014@sinano.ac.cn
Received 19 SEPTEMBER 2019; Revised 13 NOVEMBER 2019.

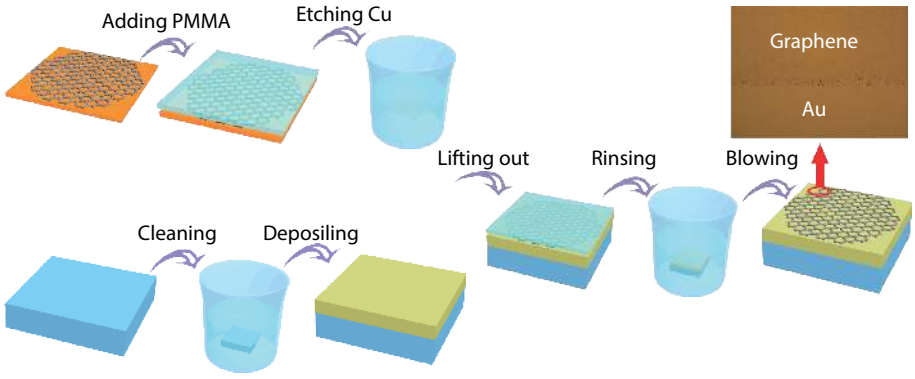

Fig. 1. (Color online) Schematic illustration of G-SAMs preparation process.

SAM exhibits an increase of modulation depth (MD) and a decrease of nonsaturable loss compared with those of the SLG-SAM. These results allow us to construct a better 1550 nm PMLFL with a threshold pump power of 60.8 mW, a pulse width of 714 fs, and a signal to noise ratio (SNR) of 62 dB.

2. Experiments and methods

As illustrated in Fig. 1, the graphene saturable absorber mirrors are fabricated on Au/Si substrates. The Au/Si substrate was achieved by depositing a 100 nm-thick Au layer on a Si substrate with the method of magnetron sputtering. Before the Au film deposition, the Si substrate was ultrasonically cleaned in organic solvents, chemically etched in 2 % HF solution, and rinsed in deionized water, blow-dried with nitrogen gas. After the growth of the Au film, SLG and TLG sheets were transferred onto the Au/Si substrates via a one-step wet chemical etching process. Each step was monitored carefully to avoid the occurrence of holes, cracks and folds of several micrometers in length into the graphene during the transfer process. The graphene is deposited on Cu foil (30 μm thick Alfa-Aesar, purity 99.99 %) by an ordinary chemical vapor deposition method. The graphene-Cu is spin-coated with Polymethyl Methacrylate (PMMA) at 500 rpm for 18 s and 3000 rpm for 60 s in sequence. The PMMA/graphene/Cu stack was then immersed in a 100 mL ammonium persulfate solution until the copper under the graphene layer was completely etched. The free-standing PMMA/graphene was then rinsed with deionized water and lifted out using the Si/Au substrate. Two samples were then baked for 15 min at 80 °C in air on a heating plate to flatten the film. Finally, the PMMA was removed using acetone and dried by nitrogen blowing.

The morphologies of SLG and TLG SAMs were characterized by optical microscope (Nikon, ECLIPSE LV100ND). An optical image of the SLG-SAM is shown in the up-right corner of Fig. 1. Surface topographies of the samples were observed by scanning electron microscope (SEM, Quanta 400 FEG). Raman spectroscopy was performed on a confocal Raman spectrometer (LABRAM HR, Japan). Nonlinear absorption characteristics of both SLG and TLG SAMs were measured by using a home-made PMLFL and the self-made Er-doped fiber amplifier (EDFA) device.

3. Results and discussion

Fig. 2 shows the SEM micrographs of SLG and TLG. The

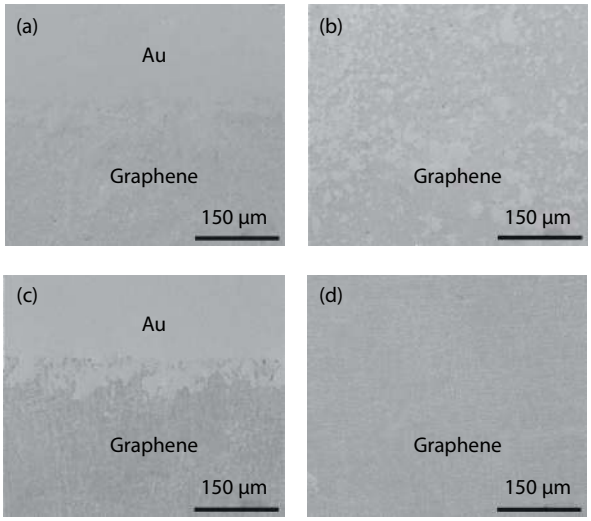

Fig. 2. The SEM micrographs of (a), (b) SLG-SAM and (c), (d) TLG-SAM.

boundary of SLG and TLG sheets transferred onto the Au films can be clearly identified in Figs. 2(a) and 2(c). Figs. 2(b) and 2(d) present SEM micrographs of the SLG- and TLG-SAMs. After the transfer process, the SLG on the Au film exhibits a lot of residues or voids, while a uniform and continuous surface in the TLG-SAM can be observed.

Raman spectroscopy is considered to be one of the main ways to study carbon materials, because it can provide information on hybridization state, defects and charged impurities[20]. As shown in Fig. 3 the Raman spectra of the graphene/Au/Si structures exhibit two major peaks from graphene, namely the G- and 2D-band. The G-band peak is located at 1580 cm^{-1}, which is attributed to the first-order Raman scattering by doubly degenerated in-plane vibration modes (in-plane optical transverse and longitudinal phonons) at the Brillouin zone centre[21, 22]. The second peak at 2700 cm^{-1} corresponds to 2D-band that is attributed to the second-order Raman scattering by in-plane transverse optical phonons near the boundary of the Brillouin zone and is closely linked to the electronic band structure. In general, the number of the graphene layer can be determined by investigating the intensity ratio of 2D and G-band (I_{2D}/I_G). The SLG SAM exhibits avalue of I_{2D}/I_G of approximately 1.82 whereas it is about 0.66 for TLG SAM, which indicates that SLG SAM has a monolayer graphene structure, and the smaller obtained I_{2D}/I_G value for TLG SAM illustrates multilayer structure in the graphene samples[23].

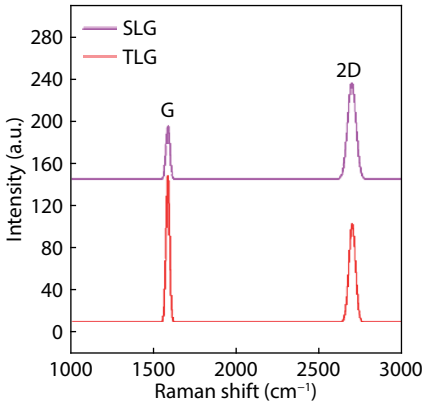

Fig. 3. (Color online) Raman spectra of SLG and TLG fabricated via a one-step transfer process.

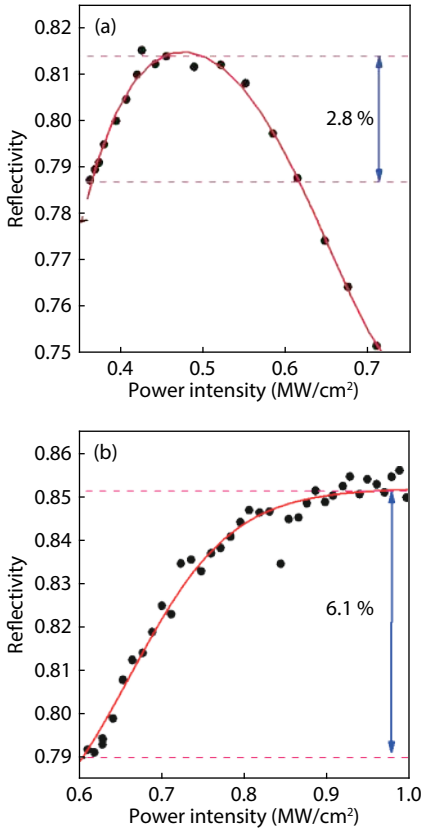

Fig. 4. (Color online) Nonlinear reflectivity curves of (a) SLG and (b) TLG SAMs.

In order to determine whether G-SAMs can be used to construct mode-locked fiber lasers at 1560 nm or not, we investigate saturable absorption properties of both SLG and TLG SAMs. A home-made PMLFL is used as a laser source, which operates at a central wavelength of 1558 nm with a pulse duration of 385 fs and a repetition rate of 21 MHz. The input power is controlled by means of a variable optical attenuator. A reference signal is employed to detect the incident power with a 1 : 1 output coupler (OC). Based on a typical balanced twin-detector measurement technology, we measured the dependence of the reflectivity of SLG and TLG SAMs on the power density of the incident pump peak, as shown in Figs. 4(a) and 4(b), respectively. The nonlinear saturable absorption properties of SLG and TLG SAMs can be expressed as[24]

$$\alpha(I) = \frac{\alpha_S}{1 + I/I_S} + \alpha_{NS},$$

where I_S is the saturation intensity (SI), α_S is the saturable absorbance and α_{NS} is the nonsaturable absorbance, respectively. The MD and SI were calculated to be approximately 2.8% and 0.41 MW/cm^2 for the SLG SAM and 6.1% and 0.66 MW/cm^2 for the TLG SAM. The increased MD and SI can be attributed to the increase of the number of graphene layers. Moreover, the nonsaturable losses of SLG and TLG SAMs are observed to be 21.2% and 20.9%. The decreased nonsaturable loss in TLG SAMs suggest the one-step wet transfer process can effectively avoid the generation of ripples or corrugations.

We have demonstrated comparative experiments by adding two G-SAMs into an Er-doped fiber laser ring cavity which was mainly comprised of laser diode of 980 nm, 980/1550 nm wavelength division multiplexer, EDF with a length of 0.8 m, polarization-independent isolator, polarization controller (PC), G-SAMs dispersion and a OC is of 10% output and 90% input. An InGaAs photoelectric converter (Thorlabs DET01CFC) converts light signals into electrical signals. The output characteristic of these fiber lasers were analyzed by using an electronic spectrum analyzer (Rohde & Schwarz FSC6), a digital oscilloscope (Rigol DS6104), and an optical spectrum analyzer (Anritsu MS9710C).

In this work, by using the TLG-SAM, a stable passively Q-switched operation is obtained at a very low pump power, which lead to the easy occurs of the mode-locked operation by gradually increasing the pump powers. Fig. 5(a) shows the measured average output power versus the input pump power of 980 nm pump laser. Before insert G-SAMs into the cavity, the lasers always operate in a continuous wave regime. When G-SAMs are inserted into the cavity, continuous wave operations started from a pump power of ~54 mW. Sable self-starting mode-locked pulse oscillations in SLG and TLG based PMLFLs are observed as pump power exceeds the threshold of 64.5 and 60.8 mW, respectively. With the increase of the pump power, the output power of both SLG and TLG based PMLFLs linearly increase corresponding to the slope efficiency is 1.7% and 2.4%, and the maximum output power SLG- and TLG-based PMLFLs is ~6.8 and 9.9 mW, respectively. The smaller lasing threshold, the larger output power, and the high slope efficiency in TLG based PMLFL suggest the nonsaturable loss of TLG-SAM is lower than that of SLG-SAM, which is well agreement with results of nonlinear characteristic measurements.

As illustrated in Fig. 5(b), the output spectrum of the SLG SAM is centered at 1557 nm with a 3-dB bandwidth of 3.0 nm and the output spectrum of the TLG SAM is centered at 1555 nm with a 3-dB bandwidth of 4.2 nm. The autocorrelation trace of the MLFL is shown in Fig. 5(e) at the threshold value. The pulse width is then obtained to be 785 fs for SLG SAM and 714 fs for TLG SAM, respectively, by autocorrelation fitting. The smaller pulse duration for TLG-based PMLFL scan be attributed to the larger MD of TLG SAMs. The time-bandwidth products (TBPs)[25] of the output pulses for both SLG- and TLG-based PMLFLs were calculated to be 0.414 and 0.526, respectively, which are quite close to the typical value of sech^2 pulse profile of 0.315[26], suggesting that the soliton is very stable with little chirp. Fig. 5(c) shows the pulse train

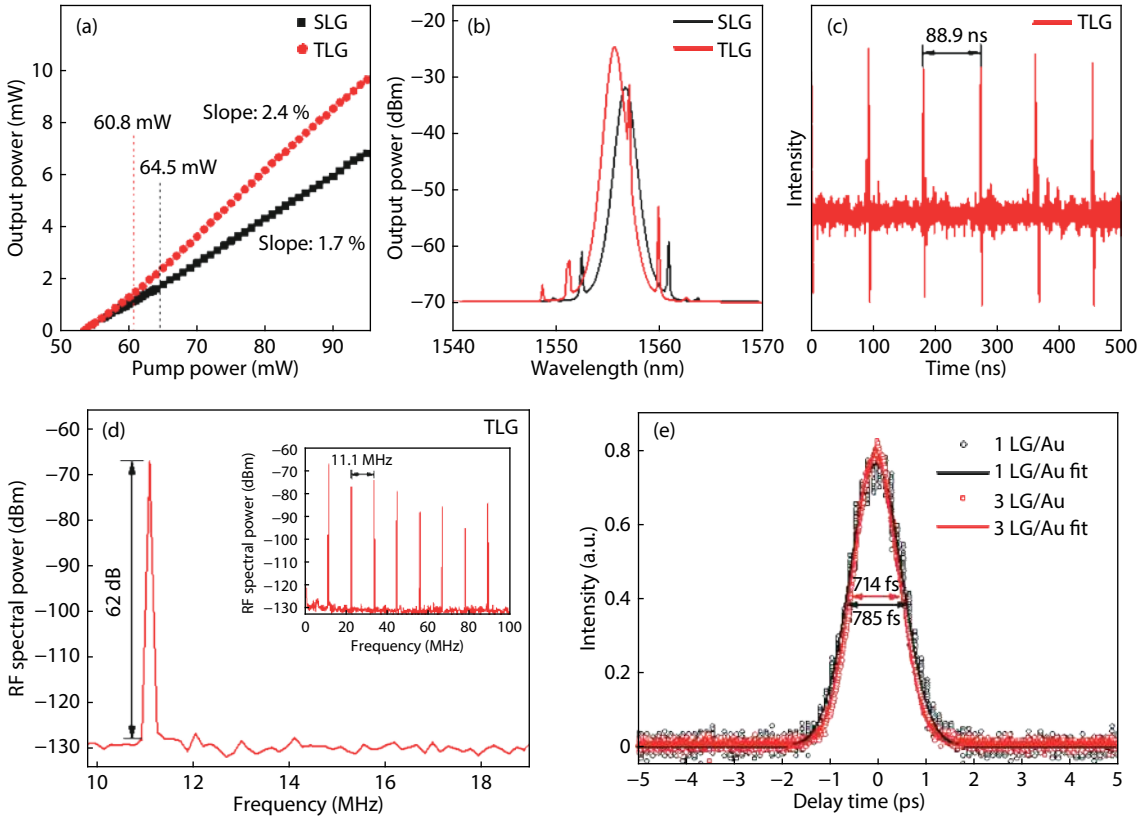

Fig. 5. (Color online) Experimental result. (a) Output power versus pump power. (b) Output optical spectra. (c) Pulse train. (d) Autocorrelation trace. (e) RF spectrum of the mode locking laser. The inset shows the broadband RF spectrum at a span of 11.1 MHz.

with a period of 88.9 ns in TLG-based PMLFL, which corresponds to the laser cavity of 24.5 m. Fig. 5(d) presents the radio frequency (RF) spectrum of the TLG-based PMLFL at the fundamental frequency peak for a scanning range of 10 MHz and RF resolution bandwidth of 100 kHz. The fundamental RF peak locates at the cavity repetition rate of 11 MHz and exhibits a signal-to-noise ratio (SNR) of 62 dB larger than that of SLG-based PMLFL, indicating TLG-SAMs have great potential to achieve stable mode-locking operation. Graphene grown on a gold film substrate by chemical vapor deposition is typically required to be transferred to another substrate for the fabrication of various graphene-based electrical, optical and mechanical devices. Therefore, the one-step transfer method reported in this work can further improve the performance of the graphene devices.

4. Conclusion

In conclusion, SLG and TLG SAMs have been fabricated by one-step wetting transfer processes. With the saturable absorption measurements, TLG SAM exhibits a larger MD and a smaller nonsaturable loss than SLG SAM due to the increased number of graphene layers and the optimized interfacial contact of the graphene with the substrate. By inserting two SAs into EDF laser cavities, a higher-performance PMLFL with a maximum output power of 9.9 mW, a slope efficiency of 2.4%, and a pulse width of 714 fs have been achieved, indicating that TLG is superior SAM candidate for PMLFLs to SLG.

Acknowledgments

This work was supported by the Key Research and Development Plan of Ministry of Science and Technology (2016YFB0402303), National Natural Science Foundation of China (NSFC) (61875222, 61605106), China Postdoctoral Science Foundation (2017M621858).

References

[1] Zhang H, Tang D Y, Zhao L M, et al. Large energy mode locking of an erbium-doped fiber laser with atomic layer graphene. Opt Express, 2009, 17(20), 17630

[2] Sun Z P, Hasan T, Torrisi F, et al. Graphene mode-locked ultrafast laser. ACS Nano, 2010, 4(2), 803

[3] Liu J J, Liu J, Guo Z N, et al. Dual-wavelength Q-switched Er:SrF_2 laser with a black phosphorus absorber in the midinfrared region. Opt Express, 2016, 24(26), 30289

[4] Lan K Y, Ker P J, Abas A F, et al. Long-term stability and sustainability evaluation for mode-locked fiber laser with graphene/PMMA saturable. Opt Commun, 2019, 435, 251

[5] Zhao L M, Tang D Y, Wu X A, et al. Dissipative soliton generation in Yb-fiber laser with an invisible intracavity bandpass filter. Opt Lett, 2010, 35(16), 2756

[6] Lu L, Liang Z M, Wu L M, et al. Few-layer bismuthene: sonochemical exfoliation, nonlinear optics and applications for ultrafast photonics with enhanced stability. Laser Photonics Rev, 2018, 12(1), 1700221

[7] Wang X, Zhu Y J, Jiang C, et al. InAs/GaAs quantum dot semiconductor saturable absorber for controllable dual-wavelength passively Q-switched fiber laser. Opt Express, 2019, 27(15), 20649

[8] Sotor J, Sobon G, Tarka J, et al. Passive synchronization of erbium and thulium doped mode-locked laser enhanced by common graphene saturable absorber. Opt Express, 2014, 22(5), 5536

[9] Martinez A, Fuse K, Xu B, et al. Optical deposition of graphene and carbon nanotubes in a fiber ferrule for passive modelocked las-

ing. Opt Express, 2010, 18(22), 23054
[10] Zhang Z Y, Oehler A E H, Resan B, et al. 1.55 μm InAs/GaAs quantum dots and high repetition rate quantum dot SESAM mode-locked laser. Sci Rep-UK, 2012, 2, 477
[11] Wang Z T, Chen Y, Zhao C J, et al. Switchable dual-wavelength synchronously Q-switched erbium-doped fiber laser based on graphene saturable absorber. IEEE Photonics J, 2012, 4(3), 869
[12] Ashoori V, Shayganmanesh M. Analytical thermal modeling of graphene-clad microfiber as a saturable absorber in ultrafast fiber lasers. Appl Phys B, 2019, 125(3), 40
[13] Zhang R L, Wang J, Liao M S, et al. Tunable Q-switched fiber laser based on a graphene saturable without additional tuning element. IEEE Photonics J, 2019, 11(1), 1500310
[14] Martinez A, Sun Z P. Nanotube and graphene saturable absorbers for fiber lasers. Nat Photonics, 2013, 7(11), 842
[15] Zhang H, Tang D Y, Knize R J, et al. Graphene mode locked, wavelength-tunable, dissipative soliton fiber laser. Appl Phys Lett, 2010, 96(11), 111112
[16] Ma J, Xie G Q, P Lv P, et al. Graphene mode-locked femtosecond laser at 2 μm wavelength. Opt Lett, 2012, 37(11), 2085
[17] Hader J, Yang H J, Scheller M, et al. Microscopic analysis of saturable absorbers: Semiconductor saturable absorber mirrors versus graphene. J Appl Phys, 2016, 119(5), 053102
[18] Bao Q L, Zhang H, Ni Z H, et al. Monolayer graphene as a saturable absorber in a mode-locked laser. Nano Res, 2011, 4(3), 297
[19] Bao Q L, Zhang H, Wang Y, et al. Atomic-layer graphene as a saturable absorber for ultrafast pulsed lasers. Adv Funct Mater, 2009, 19(19), 3077
[20] Ferrari A C. Raman spectroscopy of graphene and graphite: Disorder, electron-phonon coupling, doping and nonadiabatic effects. Solid State Commun, 2007, 143(2), 47
[21] Dresselhaus M S, Jorio A, Hofmann M. Perspectives on carbon nanotubes and graphene Raman spectroscopy. Nano Lett, 2010, 10(3), 751
[22] Zhang X, Qiao X F, Shi W, et al. Phonon and Raman scattering of two-dimensional transition metal dichalcogenides from monolayer, multilayer to bulk material. Chem Soc Rev, 2015, 44(9), 2757
[23] Botti S, Rufoloni A, Vannozzi A, et al. Investigation of CVD grown graphene topography. AIP Conf Proc, 2018, 1990
[24] Li X H, Wu K, Sun Z P, et al. Single-wall carbon nanotubes and graphene oxide-based saturable absorbers for low phase noise mode-locked fiber lasers. Sci Rep-UK, 2016, 6, 25266
[25] Luo Z Q, Li Y Y, Zhong M, et al. Nonlinear optical absorption of few-layer molybdenum diselenide ($MoSe_2$) for passively mode-locked soliton fiber laser. Photonics Res, 2015, 3(3), A79
[26] Li X H, Yu X C, Sun Z P, et al. High-power graphene mode-locked Tm/Ho co-doped fiber laser with evanescent field interaction. Sci Rep-UK, 2015, 5, 16624